ELSEVIER

Marine Geology 159 (1999) 63–78

MARINE GEOLOGY
INTERNATIONAL JOURNAL OF MARINE GEOLOGY, GEOCHEMISTRY AND GEOPHYSICS

www.elsevier.nl/locate/margeo

Variations of biogenic particle flux in the southern Atlantic section of the Subantarctic Zone during the late Quaternary: Evidence from sedimentary $^{231}Pa_{ex}$ and $^{230}Th_{ex}$

T. Asmus [a,*], M. Frank [a,1], C. Koschmieder [a,2], N. Frank [a], R. Gersonde [b], G. Kuhn [b], A. Mangini [a]

[a] *Heidelberger Akademie der Wissenschaften, INF 366, 69120 Heidelberg, Germany*
[b] *Alfred Wegener Institut für Polar- und Meeresforschung, Columbusstrasse, 27568 Bremerhaven, Germany*

Received 5 November 1997; accepted 27 November 1998

Abstract

Variations of intensity and composition of biogenic particle flux at the northern boundary of the present Polar Frontal Zone in the Atlantic sector of the Southern Ocean are indicators of major changes of paleoenvironmental conditions on glacial/interglacial time scales during the Late Quaternary. In order to estimate those past changes, sediment accumulation patterns of two piston cores, one from just north and one just south of the present day position of the Subantarctic Front were reconstructed. Using the $^{230}Th_{ex}$ method large contributions of laterally supplied material were quantified and used to correct sediment accumulation rates. During the last glacial focussing of biogenic opal-dominated material exceeded the original contribution from the surface water above by a maximum factor of 8.7. The initial activity ratio of $^{231}Pa_{ex}/^{230}Th_{ex}$ was used as tracer for biogenic particle flux and composition and indicates that during the glacial stages 2 and 4 the area of high opal productivity was situated above the location of the southern core whereas the northern core has not been reached by this northward shift during the last 130 kyr as shown by the pattern of focussing-corrected bulk accumulation rates. If the position of the Antarctic Polar Front has remained at the northern boundary of the high opal productivity area during the last 130 kyr, the results suggest that was located exactly between the two core sites during glacial stages 2 and 4. A two-box modeling approach involving particle flux and boundary scavenging intensity of ^{231}Pa was applied to estimate the possible range of the $^{231}Pa_{ex}/^{230}Th_{ex}$ ratio recorded in Southern Ocean sediments. Previous estimates on the export of ^{231}Pa from the Atlantic into the Southern Ocean are corroborated but the model suggests a low sensitivity of the $^{231}Pa_{ex}/^{230}Th_{ex}$ ratio in Southern Ocean sediments to variations of the residence time of North Atlantic Deep Water in the Atlantic Ocean.

Keywords: Th-230; Pa-231; Southern Ocean; biogenic particle flux; North Atlantic Deep Water; advection

* Corresponding author. Universität Heidelberg, Radiochemie, INF 500, 69120 Heidelberg, Germany. Fax: +49-6221-54-6082; E-mail: tasmus@ix.urz.uni-heidelberg.de

[1] Present address: University of Oxford, Department of Earth Sciences, Parks Road, Oxford OX1 3PR, UK.

[2] Present address: Universität Heidelberg, Pharmazeutische Biologie, INF 364, 69120 Heidelberg, Germany.

0025-3227/99/$ - see front matter
PII: S0025-3227(98)00199-6

1. Introduction

The Atlantic sector of the Southern Ocean is considered one of the key areas for global climate change. In particular, the knowledge of changes of biogenic particle flux and export productivity during the last climatic cycle (130 kyr B.P. until present) is important for understanding the mechanisms that led to drastic variations of ocean chemistry and nutrient availability as well as global atmospheric CO_2 concentrations. There are, however, difficulties in finding suitable and well-preserved tracers for past biogenic particle fluxes in marine sediments. The accumulation rate of organic carbon as the primary tracer may be obscured by dissolution and preservation processes and current-driven sediment redistribution. Alternatively, the Cd/Ca ratio in planktonic foraminifera may serve to derive phosphate and consequently nutrient contents of the corresponding surface water masses, which are themselves not preserved in ocean sediments (Boyle, 1988). A further tool to determine paleonutrient contents is the foraminiferal $\delta^{13}C$ ratio. In general the $\delta^{13}C$ and the Cd/Ca-methods correspond well, but in the glacial Southern Ocean the results are not in agreement. While the $\delta^{13}C$ method suggests an increase of nutrient content in glacial Antarctic surface waters (Charles and Fairbanks, 1990), the Cd/Ca ratio indicates only insignificant changes (Boyle, 1988).

The $^{231}Pa_{ex}/^{230}Th_{ex}$ activity ratio in marine sediments was suggested to represent a proxy to reveal changes in biogenic particle flux avoiding the disadvantages of the mentioned methods (Kumar et al., 1993, 1995; Francois et al., 1993, 1997). $^{231}Pa_{ex}$ and $^{230}Th_{ex}$ (ex standing for the amount of a radionuclide adsorbed onto particles from the water column) originate in the ocean water column from the ^{235}U and ^{238}U decay series with half lives of 32,500 and 75,200 years, respectively. Dissolved U is homogenously distributed in the ocean with a concentration of 3.3 μg/l (c.f. Mangini et al., 1979). Hence, the initial $^{231}Pa_{ex}/^{230}Th_{ex}$ activity ratio is 0.093. Because of the high particle reactivity of Pa and Th their mean residence time of 150 to 200 years and 5 to 40 years, respectively, is very short compared with their radioactive half lives (Nozaki et al., 1981; Anderson et al., 1983). On account of a lower particle reactivity compared with Th, Pa is not always found in the expected amount in the sediments as it is susceptible to preferential scavenging to sediments in areas with high particle fluxes, a process called boundary scavenging (Spencer et al., 1981). There, the sedimentary $^{231}Pa_{ex}/^{230}Th_{ex}$ activity ratio was observed to be higher than the expected initial ratio from radiogenic production (Anderson et al., 1983, 1990, 1994; Bacon and Anderson, 1982). As a consequence, areas with low particle fluxes yield $^{231}Pa_{ex}/^{230}Th_{ex}$ ratios lower than the production ratio. The correlation between particle flux and $^{231}Pa_{ex}/^{230}Th_{ex}$ ratio was shown to be near linear (Kumar et al., 1995). This isotope ratio is not affected by disturbing influences of dissolution of biogenic opal or carbonate or sediment redistribution. In the Atlantic Ocean enhanced boundary scavenging of ^{231}Pa is found at the coastal regions off West Africa and in the South Atlantic (Walter et al., 1997). Kumar et al. (1993) deduced a glacial northward shift of the high opal productivity area presently located south of the Antarctic Polar Front (APF) from variations of sedimentary $^{231}Pa_{ex}/^{230}Th_{ex}$ ratios. Walter et al. (1997) demonstrated that this variability may not originate from changes in particle flux alone but, due to a strong affinity of ^{231}Pa to adsorb to biogenic opal, may to a large extent be caused by alternations between periods of opal- and non-opal-dominated particle flux.

Recent results suggest that ^{231}Pa produced in the Atlantic Ocean has been transferred to the Atlantic sector of the Southern Ocean south of the actual position of the Antarctic Polar Front by deep water circulation, mainly North Atlantic Deep Water (NADW) (Yu et al., 1996). These authors also concluded that the similarly strong glacial and interglacial sink of ^{231}Pa in the southern Atlantic Ocean sediments indicates glacial NADW production and circulation as strong as during interglacials.

Two sediment cores PS2499-5 from the northern boundary of the present day position of the Polar Frontal Zone (PFZ) (46°30.7′ S, 15°20.0′ W water depth 3175 m, from the western flank of the Mid-Atlantic Ridge, about 1° south of the present position of the Subantarctic Front, SAF) and PS2498-1 (44°09.2′ S, 14°13.7′ W, water depth 3783 m, from the eastern flank of the Mid-Atlantic Ridge, about 1° north of the SAF), recovered during the ANT-XI/2 cruise of RV *Polarstern* with a recovery of 15.53 m

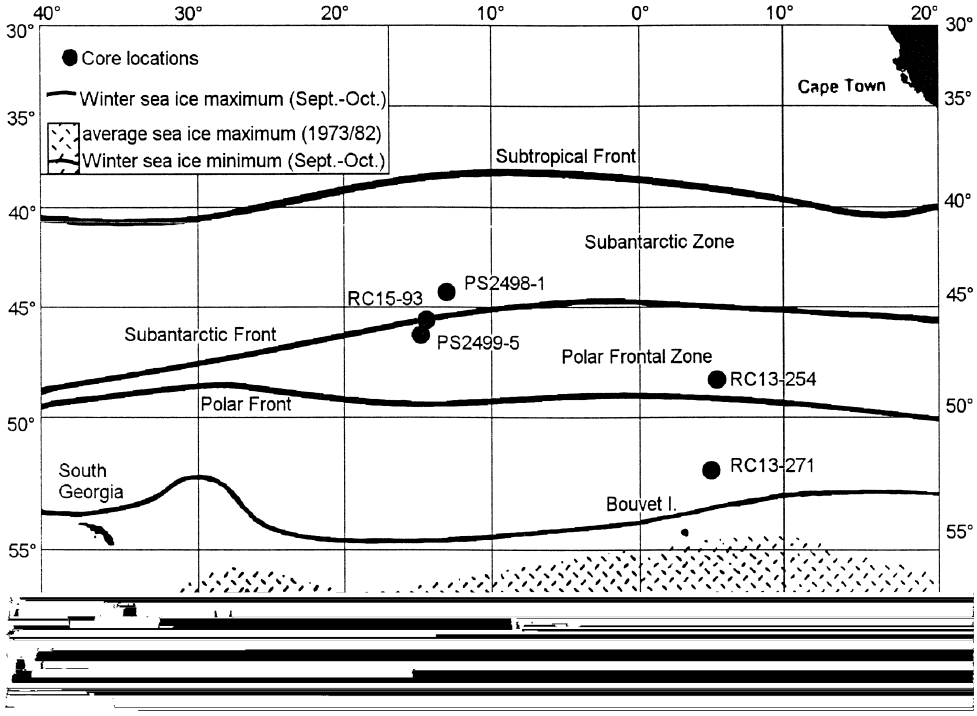

Fig. 1. Locations of the sediment cores PS2498-1, PS2499-5, RC13-271, RC13-254, RC15-93 and the frontal system in the Atlantic sector of the Southern Ocean. The present-day position of the fronts are from Peterson and Stramma (1991). The data of the sea ice distribution are from the Sea Ice Climatic Atlas (1985).

and 11.61 m, respectively, (Fig. 1, Gersonde, 1995) were chosen for this study. The SAF marks the boundary between the Sub Antarctic Zone (SAZ) and the PFZ and is characterized by high gradients of density, salinity, nutrient concentrations and temperature (c.f. Peterson and Stramma, 1991, Fig. 1). At present, the lithologies of both sediment cores are dominated by biogenic carbonate sedimentation, indicating a lower surface water productivity than in the opal-dominated high biogenic particle flux areas presently located mainly south of the APF (Kumar et al., 1993, 1995; Frank, 1996). Whereas core PS2499-5 shows a downcore alternation between biogenic opal and carbonate, core PS2498-1 is dominated by carbonate throughout. The stratigraphy of core PS2499-5 was established applying the $\delta^{18}O$ method using planktonic foraminiferal species (*G. bulloides* and *N. pachyderma sin.*) and benthic foraminifers in combination with lithostrathigraphic (carbonate and biogenic opal) and biostratigraphic methods. The stratigraphy of the PS2498-1 is based on $\delta^{18}O$ (*N. pachyderma sin.*). These stratigraphic data will be published separately together with the opal and carbonate data.

The motivation for the application of the radionuclide tracer methods to these two cores were their locations north and south of the Subantarctic Front and their water depths above the CCD. This implies a potential to sensitively record any paleoenvironmental changes at this location during the last about 130 kyr, such as shifts of the high biogenic particle flux area related to glacial/interglacial climatic conditions similar to investigations of Kumar et al. (1993) at the position of the APF further south.

2. Analytical methods

To determine the ^{231}Pa activity via α spectroscopy, the Pa of the sediment samples was chemically separated and then electrodeposited on stainless steel plates. A detailed description of this method,

Table 1
PS2499-5: core depth and corresponding age, initial $^{231}Pa_{ex}$, initial $^{230}Th_{ex}$, and $^{231}Pa_{ex}/^{230}Th_{ex}$

Depth (cm)	Age (kyr)	$^{231}Pa_{ex}$ (dpm/g)	$^{230}Th_{ex}$ (dpm/g)	$^{231}Pa_{ex}/^{230}Th_{ex}$
4	3.01	0.72±0.06	8.06±0.31	0.089±0.01
15	5.87	0.68±0.03	8.00±0.33	0.085±0.01
25	8.36	0.69±0.03	7.90±0.40	0.087±0.01
35	10.47	0.79±0.04	8.99±1.17	0.088±0.01
45	11.90	0.80±0.06	7.67±0.46	0.104±0.01
57	12.46	0.97±0.13	6.20±0.52	0.157±0.02
86	12.90	0.90±0.11	4.15±0.49	0.217±0.04
116	13.31	0.65±0.07	3.99±0.20	0.162±0.02
146	13.71	0.72±0.08	3.63±0.34	0.198±0.03
177	14.18	0.72±0.08	4.03±0.41	0.178±0.03
207	14.74	0.56±0.06	3.71±0.27	0.151±0.02
246	15.27	0.55±0.05	3.96±0.36	0.139±0.02
277	15.68	0.56±0.06	3.31±0.32	0.168±0.02
317	16.03	0.52±0.05	2.90±0.44	0.177±0.03
346	16.37	0.55±0.04	3.42±0.32	0.162±0.02
377	16.80	0.86±0.08	4.45±0.80	0.193±0.04
407	17.24	0.59±0.05	3.90±0.37	0.152±0.02
446	17.68	0.27±0.03	3.51±0.63	0.077±0.02
477	18.27	0.76±0.06	4.18±0.42	0.180±0.02
517	18.64	0.46±0.06	2.92±0.54	0.157±0.03
546	19.01	0.36±0.04	3.23±0.35	0.112±0.02
577	19.41	0.70±0.07	3.80±0.39	0.185±0.03
607	19.98	0.38±0.04	4.54±0.41	0.084±0.01
646	20.55	0.67±0.06	4.35±0.26	0.153±0.02
675	21.00	0.49±0.06	4.55±0.38	0.108±0.02
697	21.25	0.37±0.04	3.42±0.57	0.109±0.02
717	21.62	0.54±0.03	4.09±0.46	0.131±0.02
746	22.00	0.56±0.06	4.10±0.33	0.137±0.02
767	22.29	0.53±0.09	4.16±0.61	0.128±0.03
787	22.56	0.56±0.04	3.16±0.50	0.178±0.03
817	23.04	0.69±0.07	3.97±0.34	0.175±0.02
846	23.45	0.85±0.10	3.84±0.45	0.222±0.04
875	23.93	0.60±0.06	3.84±0.36	0.155±0.02
916	26.70	0.50±0.05	4.35±0.28	0.115±0.01
946	29.15	0.63±0.05	4.76±0.55	0.132±0.02
966	31.04	0.55±0.04	3.89±0.24	0.141±0.01
996	35.01	0.65±0.09	5.35±0.50	0.121±0.02
1026	37.18	0.51±0.08	3.85±0.50	0.133±0.03
1046	40.96	0.53±0.06	6.11±0.48	0.086±0.01
1076	43.90	0.37±0.08	4.85±0.54	0.077±0.02
1097	46.93	0.22±0.07	4.86±0.50	0.046±0.01
1126	50.49	0.70±0.12	5.72±0.57	0.122±0.02
1146	53.46	0.85±0.06	5.65±0.38	0.151±0.02
1168	55.26	0.76±0.09	3.24±0.65	0.236±0.05
1198	58.88	0.83±0.13	5.42±0.59	0.154±0.03
1228	60.77	0.67±0.08	3.92±0.55	0.171±0.03
1245	62.18	0.57±0.07	3.46±0.44	0.164±0.03
1269	64.53	0.87±0.11	3.98±0.72	0.218±0.05
1299	66.79	0.48±0.09	3.86±0.54	0.125±0.03
1324	69.13	0.49±0.12	4.55±0.62	0.107±0.03
1346	71.65	0.78±0.10	4.91±0.57	0.158±0.03
1368	73.99	0.76±0.12	4.93±0.73	0.154±0.03
1388	80.50	0.83±0.11	7.17±0.66	0.116±0.02
1407	86.34	1.04±0.13	7.28±0.50	0.143±0.02
1417	91.00	0.66±0.11	6.21±0.44	0.106±0.02
1438	103.70	0.87±0.17	11.99±1.07	0.072±0.02
1457	108.21	0.81±0.16	6.86±0.95	0.117±0.03
1467	112.87	0.68±0.17	9.62±1.11	0.071±0.02
1477	117.68	0.44±0.16	8.29±1.12	0.054±0.02
1487	123.27	0.39±0.17	7.71±0.60	0.050±0.02
1497	129.51	1.64±0.49	10.51±1.65	0.156±0.05

The error represents one standard deviation of the mean (1 σ).

first applied to Mn/Fe crusts is given by Frank and Mangini (1995) and is in this study for the first time applied to marine sediments. Every sample was dried and homogenized. Then an α ^{233}Pa spike was added to 0.5–2.0 g of material. This ^{233}Pa spike addition was necessary, because the yield of the chemical separation procedure varies between 40 and 90%. The ^{233}Pa spike was produced at the DKFZ Heidelberg. After treatment with HF and heating until dryness twice, melting with $LiBO_2$ followed for total dissolution of the sample in 8 N HCl. To separate the largest part of Ca, a solution of $FeCl_3$ was added and the Pa was coprecipitated with iron hydroxide by adding an excess of NH_3. After 10 h the remaining residue was separated, washed, dried and dissolved in hot 8 N HCl. Pa was then separated via ion exchange columns in several eluation steps (Frank and Mangini, 1995). The final solution was treated with HCl and HNO_3 to destroy Pa complexes, heated until dryness, redissolved and buffered. Finally, electrodeposition on stainless steel plates took place to measure the α and β activity.

Excess ^{231}Pa originating from the water column is obtained after subtraction of supported ^{231}Pa activities, since ^{231}Pa also originates from authigenic and lithogenic U sources in the sediment. The correction was carried out according to the following equation (Francois et al., 1993):

$$^{231}Pa_{ex} = {}^{231}Pa_{total} - {}^{231}Pa_{lith} - {}^{231}Pa_{auth} \quad (1)$$

Table 2
PS2499-5: age, mean sedimentation rate, ^{230}Th constant flux sedimentation rate, bulk SAR and rain rate

Age (kyr)	Mean sed. rate (cm/kyr)	Const. flux sed. rate (cm/kyr)	Sed. acc. rate (g/cm^2 kyr)	Rain rate (g/cm^2 kyr)
3.01	4.17	3.65	2.45±0.09	1.04±0.04
5.87	4.17	3.68	2.46±0.10	1.04±0.04
8.36	4.17	4.01	2.49±0.13	1.06±0.05
10.47	4.17	4.73	2.18±0.28	0.93±0.12
11.90	4.17	7.68	2.54±0.15	1.09±0.06
12.46	70.83	36.88	11.80±0.99	1.35±0.11
12.90	70.83	67.68	17.60±2.08	2.01±0.24
13.31	70.83	73.24	18.31±0.93	2.09±0.11
13.71	70.83	74.64	20.15±1.91	2.30±0.22
14.18	70.83	64.77	18.13±1.85	2.07±0.21
14.74	70.83	61.71	19.75±1.44	2.25±0.16
15.27	70.83	65.91	18.45±1.67	2.11±0.19
15.68	70.83	88.23	22.06±2.14	2.52±0.24
16.03	70.83	96.79	25.16±3.77	2.88±0.43
16.37	70.83	88.87	21.33±1.97	2.44±0.22
16.80	70.83	71.41	16.43±2.96	1.88±0.34
17.24	70.83	78.03	18.73±1.79	2.14±0.20
17.68	70.83	80.09	20.82±3.76	2.38±0.43
18.27	70.83	60.33	17.49±1.75	2.00±0.20
18.64	70.83	92.54	24.99±4.59	2.86±0.52
19.01	70.83	80.67	22.59±2.47	2.58±0.28
19.41	70.83	76.97	19.24±1.95	2.20±0.22
19.98	70.83	59.73	16.13±1.46	1.84±0.17
20.55	70.83	60.05	16.82±1.00	1.92±0.11
21.00	70.83	57.36	16.06±1.33	1.83±0.15
21.25	70.83	82.02	21.32±3.53	2.44±0.40
21.62	70.83	66.23	17.88±2.01	2.04±0.23
22.00	70.83	65.94	17.80±1.45	2.03±0.17
22.29	70.83	70.27	17.57±2.58	2.01±0.29
22.56	70.83	92.43	23.11±3.64	2.64±0.42
23.04	70.83	61.33	18.40±1.58	2.10±0.18
23.45	70.83	70.45	19.02±2.22	2.17±0.25
23.93	70.83	73.27	19.05±1.78	2.18±0.20
26.70	8.57	12.81	3.59±0.23	1.92±0.12
29.15	8.57	10.21	3.27±0.37	1.75±0.20
31.04	8.57	13.25	3.98±0.25	2.15±0.13
35.01	8.57	7.56	2.95±0.28	1.56±0.15
37.18	8.57	11.52	4.03±0.52	2.17±0.28
40.96	8.57	6.61	2.58±0.20	1.37±0.11
43.90	8.57	8.70	3.22±0.36	1.72±0.19
46.93	8.57	8.25	3.22±0.33	1.72±0.18
50.49	8.57	6.87	2.75±0.27	1.46±0.15
53.46	8.57	7.09	2.76±0.19	1.48±0.10
55.26	8.57	14.45	4.77±0.95	2.58±0.51
58.88	8.57	8.29	2.90±0.32	1.54±0.17
60.77	11.33	12.43	3.48±0.49	2.13±0.30
62.18	11.33	14.52	3.92±0.49	2.41±0.30
64.53	11.33	11.47	3.44±0.62	2.10±0.38
66.79	11.33	12.21	3.54±0.49	2.16±0.30
69.13	11.33	10.02	3.01±0.41	1.83±0.25
71.65	11.33	8.74	2.80±0.32	1.70±0.20
73.99	11.33	8.97	2.78±0.41	1.69±0.25
80.50	2.41	3.00	1.32±0.12	1.16±0.11
86.34	2.41	2.48	1.29±0.09	1.15±0.08
91.00	2.41	3.32	1.50±0.11	1.34±0.10
103.70	2.41	1.57	0.83±0.07	0.70±0.06
108.21	2.41	3.22	1.35±0.19	1.22±0.17
112.87	2.41	2.15	0.97±0.11	0.87±0.10
117.68	2.41	2.08	1.12±0.15	1.01±0.14
123.27	2.41	1.79	1.22±0.09	1.08±0.08
129.51	2.41	1.60	0.90±0.14	0.79±0.12

The error represents one standard deviation of the mean (1 σ).

equivalent to:

$$^{231}\mathrm{Pa}_{ex} = {}^{231}\mathrm{Pa}_{total} - {}^{235}\mathrm{U}_{lith} - \left({}^{235}\mathrm{U}_{total} - {}^{235}\mathrm{U}_{lith}\right) \times \left(1 - \exp\left(-\lambda\left({}^{231}\mathrm{Pa}\right)t\right)\right)$$

$$^{231}\mathrm{Pa}_{ex} = {}^{231}\mathrm{Pa}_{total} - {}^{232}\mathrm{Th}\cdot 0.0338 - \left(0.045\cdot {}^{238}\mathrm{U} - {}^{232}\mathrm{Th}\cdot 0.0338\right) \times \left(1 - \exp\left(-\lambda\left({}^{231}\mathrm{Pa}\right)t\right)\right) \quad (2)$$

with:

$^{231}\mathrm{Pa}_{ex}$ activity of the ^{231}Pa in dpm/g, originating from the water column from dissolved ^{235}U, removed by particles to the sediment

$^{231}\mathrm{Pa}_{total}$ activity of the ^{231}Pa in dpm/g, measured by α spectroscopy

$^{231}\mathrm{Pa}_{lith}$ activity of the ^{231}Pa in dpm/g, originating from the detrital ^{235}U in the particles themselves, $^{231}\mathrm{Pa}_{lith} = {}^{235}\mathrm{U}_{lith} = {}^{232}\mathrm{Th}\cdot 0.0338$

$^{231}\mathrm{Pa}_{auth}$ activity of the ^{231}Pa in dpm/g, originating from ^{235}U, which diffused into the sediment after sedimentation due to pore water gradients caused by underlying reduced sediment sections 2 $^{231}\mathrm{Pa}_{auth} = {}^{235}\mathrm{U}_{auth}(1 - \exp(-\lambda(^{231}\mathrm{Pa})t))$

$^{232}\mathrm{Th}$ measured activity of the ^{232}Th in dpm/g

Table 3
PS248-1: core depth and corresponding age, initial $^{230}Th_{ex}$, mean sedimentation rate, ^{230}Th constant flux sedimentation rate, bulk SAR and rain rate

Mean depth (cm)	Age (kyr)	$^{230}Th_{ex}$ (dpm/g)	Mean sed. rate (cm/kyr)	Const. flux sed. rate (cm/kyr)	Sed. acc. rate (g/cm^2 kyr)	Rain rate (g/cm^2 kyr)
9	2.13	9.54 ± 0.46	8.33	8.45 ± 0.41	6 ± 0.29	1.04 ± 0.05
20	2.64	10 ± 0.43	8.33	7.84 ± 0.33	5.64 ± 0.24	1 ± 0.04
36	5.8	9.2 ± 0.61	8.33	8.85 ± 0.58	6.29 ± 0.41	1.08 ± 0.07
62.5	8.86	10.53 ± 0.37	8.33	8.18 ± 0.28	5.48 ± 0.19	0.94 ± 0.03
80	9.97	11.5 ± 0.55	8.33	8.97 ± 0.43	4.93 ± 0.24	0.86 ± 0.04
90	10.96	12.17 ± 0.66	8.33	10.13 ± 0.55	4.66 ± 0.25	0.82 ± 0.04
100	12.01	12.89 ± 0.56	9.38	9.56 ± 0.42	4.4 ± 0.19	0.77 ± 0.03
110	13.4	11.13 ± 0.54	9.38	7.2 ± 0.35	3.38 ± 0.17	0.89 ± 0.04
120	14.36	7.69 ± 0.51	9.38	10.38 ± 0.69	4.88 ± 0.32	1.29 ± 0.09
137.5	16.65	7.72 ± 0.57	9.38	10.92 ± 0.81	4.91 ± 0.36	1.29 ± 0.1
162.5	19.13	8.77 ± 0.49	9.38	10.08 ± 0.56	4.33 ± 0.24	1.13 ± 0.06
187.5	21.32	7.91 ± 0.58	9.38	11.41 ± 0.84	4.79 ± 0.35	1.26 ± 0.09
212.5	24	9.73 ± 0.47	9.38	9.32 ± 0.45	3.92 ± 0.19	1.02 ± 0.05
237.5	25.54	8.96 ± 0.48	13.57	16.23 ± 0.87	6.98 ± 0.37	1.11 ± 0.06
262.5	27.07	8.7 ± 0.4	13.57	16.33 ± 0.76	7.19 ± 0.33	1.14 ± 0.05
287.5	28.62	9.02 ± 0.44	13.57	16.13 ± 0.78	6.93 ± 0.34	1.1 ± 0.05
312.5	30.03	7.62 ± 0.29	13.57	17.83 ± 0.68	8.2 ± 0.32	1.31 ± 0.05
337.5	31.52	7.97 ± 0.37	13.57	16.7 ± 0.77	7.85 ± 0.36	1.25 ± 0.06
362.5	33.34	8.63 ± 0.36	13.57	13.72 ± 0.58	7.27 ± 0.31	1.15 ± 0.05
387.5	35.43	9.55 ± 0.37	13.57	11.96 ± 0.46	6.58 ± 0.25	1.04 ± 0.04
412.5	37.4	8.81 ± 0.38	13.57	12.73 ± 0.55	7.13 ± 0.31	1.13 ± 0.05
437.5	39.21	8.25 ± 0.39	13.57	13.82 ± 0.65	7.6 ± 0.36	1.21 ± 0.06
462.5	40.85	7.36 ± 0.32	13.57	15.19 ± 0.66	8.51 ± 0.37	1.35 ± 0.06
487.5	42.63	7.98 ± 0.48	13.57	14.04 ± 0.84	7.86 ± 0.47	1.25 ± 0.07
512.5	44.54	9.04 ± 0.44	13.57	13.09 ± 0.64	6.94 ± 0.34	1.1 ± 0.05
537.5	46.85	10.22 ± 0.42	13.57	10.82 ± 0.44	6.17 ± 0.25	0.97 ± 0.04
562.5	48.84	8.92 ± 0.46	13.57	12.58 ± 0.64	7.04 ± 0.36	1.12 ± 0.06
587.5	50.75	8.56 ± 0.41	13.57	13.1 ± 0.62	7.34 ± 0.35	1.16 ± 0.06
612.5	52.69	8.72 ± 0.47	13.57	12.86 ± 0.69	7.2 ± 0.39	1.14 ± 0.06
637.5	54.67	8.85 ± 0.44	13.57	12.67 ± 0.63	7.1 ± 0.35	1.12 ± 0.06
662.5	56.58	9.23 ± 0.46	13.57	13.08 ± 0.65	6.8 ± 0.34	1.08 ± 0.05
687.5	58.58	9.86 ± 0.56	13.57	12.49 ± 0.71	6.37 ± 0.36	1.01 ± 0.06
712.5	63.82	12.01 ± 0.33	6.43	4.77 ± 0.13	2.57 ± 0.07	0.83 ± 0.02
737.5	67.69	8.9 ± 0.4	6.43	6.47 ± 0.29	3.43 ± 0.15	1.12 ± 0.05
762.5	71.13	7.91 ± 0.52	6.43	7.25 ± 0.47	3.84 ± 0.25	1.26 ± 0.08
784	73.81	8.8 ± 0.48	6.43	6.73 ± 0.37	3.43 ± 0.19	1.13 ± 0.06
805.5	76.63	9.75 ± 0.51	6.57	8.87 ± 0.46	5.15 ± 0.27	1.02 ± 0.05
830.5	80.38	11.53 ± 0.55	6.57	6.65 ± 0.31	4.39 ± 0.21	0.86 ± 0.04
855.5	83.74	10.74 ± 0.37	6.57	7.46 ± 0.26	4.7 ± 0.16	0.93 ± 0.03
880.5	87.31	10.47 ± 0.39	6.57	6.99 ± 0.26	4.83 ± 0.18	0.95 ± 0.04
905.5	90.56	9.1 ± 0.92	6.57	7.69 ± 0.78	5.54 ± 0.56	1.09 ± 0.11
930.5	94.65	13.38 ± 0.8	6.57	6.12 ± 0.36	3.8 ± 0.23	0.74 ± 0.04
955.5	98.9	13.33 ± 0.88	6.57	5.87 ± 0.39	3.82 ± 0.25	0.75 ± 0.05
980.5	103.36	13.35 ± 0.53	6.57	5.61 ± 0.22	3.82 ± 0.15	0.75 ± 0.03
1005.5	106.88	10.63 ± 0.58	6.57	7.09 ± 0.39	4.75 ± 0.26	0.94 ± 0.05
1030.5	110.96	12.34 ± 0.52	6.57	6.14 ± 0.26	4.11 ± 0.17	0.81 ± 0.03
1055.5	115.37	14.06 ± 1.05	6.57	5.66 ± 0.42	3.62 ± 0.27	0.71 ± 0.05
1080.5	120.24	14.02 ± 0.49	6.57	5.14 ± 0.18	3.65 ± 0.13	0.71 ± 0.02

Table 3 (continued)

Mean depth (cm)	Age (kyr)	$^{230}Th_{ex}$ (dpm/g)	Mean sed. rate (cm/kyr)	Const. flux sed. rate (cm/kyr)	Sed. acc. rate (g/cm^2 kyr)	Rain rate (g/cm^2 kyr)
1105.5	123.95	10.57 ± 0.63	6.57	6.74 ± 0.4	4.79 ± 0.29	0.94 ± 0.06
1130.5	126.31	6.74 ± 0.89	6.57	10.59 ± 1.41	7.41 ± 0.98	1.48 ± 0.2
1152	128.43	7.84 ± 0.89	6.57	8.48 ± 0.96	6.36 ± 0.72	1.27 ± 0.14

The error represents one standard deviation of the mean (1 σ).

0.0338	ratio of the $^{235}U/^{232}Th$ activity, $^{235}U/^{232}Th = 0.0338 \pm 0.0113$
0.045	ratio of the $^{235}U/^{238}U$ activity, $^{235}U/^{238}U = 0.045$
^{238}U	measured activity of the ^{238}U in dpm/g
$\lambda(^{231}Pa)$	decay constant of ^{231}Pa, $\lambda(^{231}Pa) = 2.13 \times 10^{-5}$ y^{-1}
t	sample age in years

^{230}Th, ^{238}U and ^{235}U activities were determined in a similar way as described by Frank et al. (1994) via α spectroscopy.

3. Results and discussion

Depth profiles of initial $^{231}Pa_{ex}$ and $^{230}Th_{ex}$ activities of cores PS2499-5 (Tables 1 and 2) and PS2498-1 (Table 3) are plotted in Fig. 2. The $^{230}Th_{ex}$ activity profiles of both cores show pronounced maxima during isotope stages 5 and 1. The ^{231}Pa activity, in contrary, does not show any significant features related to glacial/interglacial changes.

In order to derive realistic sediment accumulation rates and fluxes of ^{231}Pa from these data in a regime such as the Antarctic Circumpolar Current (ACC) with high bottom current velocities, lateral sediment redistribution has to be quantified. Driven by bottom currents, sinking particles, loaded with $^{230}Th_{ex}$ may be laterally removed (winnowing) to be deposited elsewhere (focussing). In addition, resuspension and redeposition of surface sediments may occur. Assuming that all the $^{230}Th_{ex}$ produced in the water column is deposited in the sediments below due to its high particle reactivity, the flux of $^{230}Th_{ex}$ to the sediments is expected to match its production rate. Any observed significant deviations from this constant flux are attributed to sediment redistribution effects. Hence, by calculating the ratio between the measured and the expected $^{230}Th_{ex}$ accumulation rate (focussing factor) these effects can be quantified. By dividing the bulk sediment accumulation rate (SAR) ($^{230}Th_{ex}$ constant flux-derived sedimentation rate multiplied by dry bulk density) by the focussing factor, rain rates are calculated, which represent sediment redistribution-corrected accumulation rates (c.f. Francois et al., 1993; Kumar et al., 1993, 1995; Frank et al., 1996). This calculation may be biased by an additional advective contribution of ^{230}Th from the Weddell Sea (Rutgers van der Loeff and

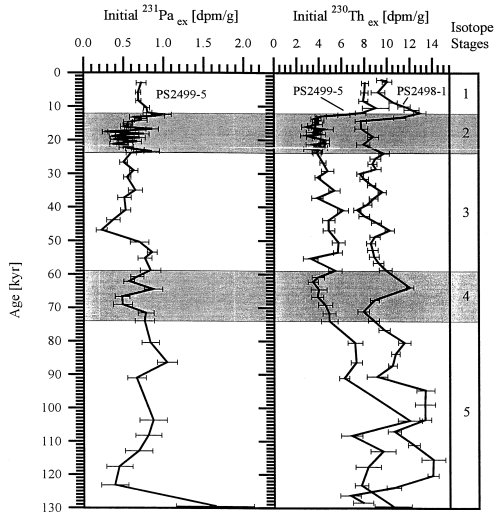

Fig. 2. Initial $^{231}Pa_{ex}$ and $^{230}Th_{ex}$ activities [dpm/g] vs. age [kyr] for core PS2499-5 and $^{230}Th_{ex}$ activity for core PS2498-1 vs. age. The error bars mark the standard deviation of the mean (1 σ). The shaded areas mark the glacial stages 2 and 4.

Berger, 1993) which may result in a slight underestimation of the rain rates. Another potential bias may arise from the lateral supply of sediments originating from shallower water depths which have experienced lower $^{230}Th_{ex}$ fluxes. In the case of the two cores of this study this is negligible because they were recovered relatively close and not much deeper than the crest of the Mid Atlantic Ridge which would be the only possible source of sediments from slightly shallower water depths. Potential effects disturbing the application of the $^{230}Th_{ex}$ constant flux model were discussed in detail in Frank et al. (1996) where it was concluded that the maximum deviation from a constant flux due to these effects may be about 50%. Any deviations from a constant flux above 50% must be attributed to sediment redistribution.

In Fig. 3 the SAR is compared to the rain rate of the two cores. In core PS2499-5 a high focussing factor of 8.7 for the opal sediments of the last glacial period led to a high SAR of up to 25 g/cm^2 kyr. A factor of around 2.4 for isotope stage 1 and a factor of around 1.9 and 1.6 for the isotope stages 3 and 4 is observed, while during the rest of the last 130 kyr sediment focussing was not significant. At the location of core PS2498-1 sediment focussing occurred during the whole period of the last 130 kyr. Maxima

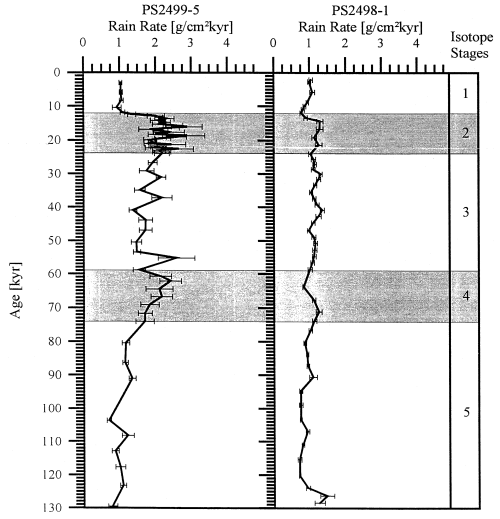

Fig. 4. Rain rate profiles of the cores PS2498-1 and PS2499-5 [g/cm^2 kyr] vs. age. The error bars mark the standard deviation of the mean (1 σ) of the $^{230}Th_{ex}$ activities. The shaded areas mark the glacial stages 2 and 4.

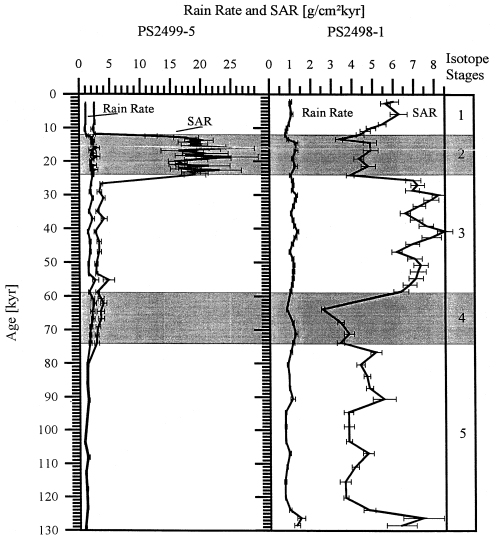

Fig. 3. Sediment accumulation rates (SAR) [g/cm^2 kyr] of the cores PS2498-1 and PS2499-5 compared with the sediment redistribution corrected rain rate vs. age. The error bars mark the standard deviation of the mean (1 σ) of the $^{230}Th_{ex}$ activities. The shaded areas mark the glacial stages 2 and 4.

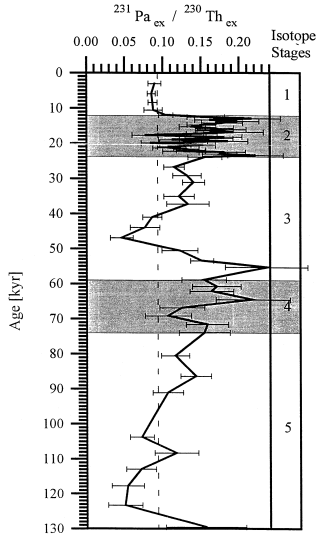

Fig. 5. Initial $^{231}Pa_{ex}$ /$^{230}Th_{ex}$ ratios of the core PS2499-5 vs. age (kyr). The dashed line indicates the ratio expected from the production rate of the two radionuclides in the water column. The error bars mark the standard deviation of the mean (1 σ). The shaded areas mark the glacial stages 2 and 4.

are found during isotope stage 1 (factor 5.7) and isotope stage 3 (factor 6.3) and isotope stage 5 (factor 5). The influence of opal dissolution on the sediments of this core was probably moderate. Following the estimate of Broecker and Peng (1982) of the opal dissolution rate in marine sediments, opal in PS 2498-1 should be well preserved (> 50%) because of the high bulk sediment accumulation rate between 5 and 8 g/cm^2 kyr throughout the core.

The rain rates of both cores show a much smaller variability than the SARs (Fig. 4). In core PS2499-5 values between 2 and 2.9 g/cm^2 kyr during the glacial stages 2, 3 and during stage 4 compared to values around 1 for the interglacial stage 5 and 1. In core PS2498-1 the rain rate shows no significant variations from 1 g/cm^2 kyr in the whole core while there is a trend towards slightly higher values during the isotope stages 2 to 4. At the very beginning of isotope stage 5 a slight maximum may also be due to disturbances caused by the proximity to the bottom of core. This suggests that there have only been very minor changes in particle flux at this location.

In order to evaluate the variations of the biogenic particle flux, the initial $^{231}Pa_{ex}/^{230}Th_{ex}$ ratios of core PS2499-5 were determined (Fig. 5). This isotope ratio was shown to generally correlate to bulk particle flux (c.f. Kumar et al., 1995) which represents a reasonable approach to evaluate biogenic particle flux in this study because the lithologies of both cores are dominated by biogenic carbonate and opal. Contributions by terrigenous material are small. Maxima of the $^{231}Pa_{ex}/^{230}Th_{ex}$ ratio around 0.2 during the glacial stages 2 and 4 and also at the beginning of stage 3, which exceed the value of 0.093 expected from production (Fig. 5) coincide with periods of increased sediment rain rates (Fig. 4). Those $^{231}Pa_{ex}/^{230}Th_{ex}$ maxima were caused by increased biogenic particle fluxes and productivity

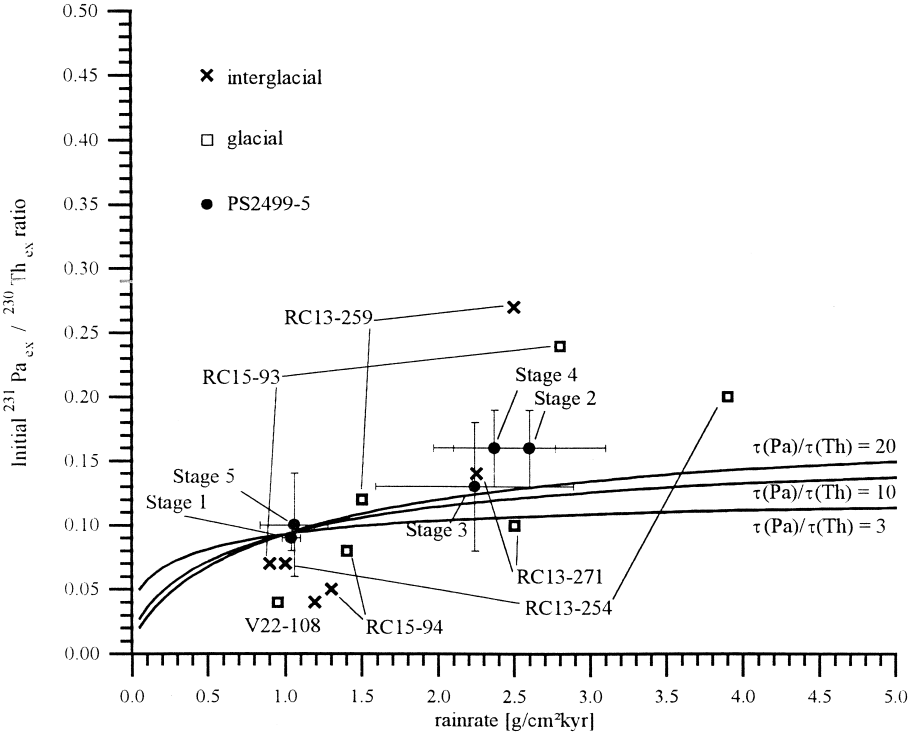

Fig. 6. Average $^{231}Pa_{ex}/^{230}Th_{ex}$ ratios for the isotope stages 1 to 5 of sediment core PS2499-5 (circles), glacial (boxes) and interglacial (crosses) $^{231}Pa_{ex}/^{230}Th_{ex}$ ratios of several sediment cores (Kumar et al., 1995), plotted against bulk sediment rain rate.

Table 4
Latitude, glacial rain rates and glacial $^{231}Pa_{ex}/^{230}Th_{ex}$ ratios of several sediment cores (Kumar et al., 1995)

Core	Latitude (°)	Glacial rain rate (g/cm^2 kyr)	Glacial $^{231}Pa_{ex}/^{230}Th_{ex}$
RC15-94	42.9	1.4	0.08
V22-108	43.18	0.95	0.04
PS2498-1	44.15	1.1	–
RC15-93	46.1	2.8	0.24
PS2499-5	46.51	2.6	0.16
RC13-254	48.57	3.9	0.2
RC13-271	51.98	2.5	0.1
RC13-259	53.88	1.5	0.12

and an increased scavenging intensity of ^{231}Pa caused by higher opal to carbonate ratios (Luo and Ku, 1996, Walter et al., 1997).

During isotope stages 5, 3 and 1 biogenic particle fluxes were greatly diminished and, as suggested by $^{231}Pa_{ex}/^{230}Th_{ex}$ ratios below 0.093, even an export of ^{231}Pa occurred. To compare the measured initial $^{231}Pa_{ex}/^{230}Th_{ex}$ ratios of the core investigated here with data of former investigations we plotted available values against the corresponding rain rates in Fig. 6 (Table 4). In spite of a large uncertainty and the changing opal to carbonate ratios the plot shows an increase of the $^{231}Pa_{ex}/^{230}Th_{ex}$ ratio with the rain rate.

4. The relationship between $^{231}Pa_{ex}/^{230}Th_{ex}$ ratio and sedimentation

The observed glacial $^{231}Pa_{ex}/^{230}Th_{ex}$ ratio and the rain rates in the zone of high productivity and the open ocean during isotope stage 2 may be related according to a simple two-box model described by Broecker and Peng (1982) and recently applied by Rutsch et al. (1995). The ocean residence times of the tracer metals are assumed to be approximately of the same order of magnitude as the mixing time of the ocean. In this two-box model one box represents the open ocean (Atlantic Ocean) and the other one a coastal region or any other zone of high productivity (SOC) where a higher particle flux and enhanced trace metal scavenging take place (Fig. 7). Constant glacial boundary scavenging in that zone is assumed because of the relatively large mean water residence time therein according to Rutgers van der Loeff and Berger (1993). A trace metal's ratio R of coastal to open ocean flux density can be described by the following equations:

$$R = \frac{F_c}{F_o} = \frac{1 + \dfrac{n}{(1-a)s}}{1 + \dfrac{n}{(1-s)a}} \tag{3}$$

with F_c: coastal flux density of the metal in dpm/cm^2 kyr; F_o: open ocean flux density of the metal in dpm/cm^2 kyr

$$a = V_o/V = A_o/A \tag{4}$$

with V: total volume of the two boxes; V_o: volume of the open ocean; A: total surface of the two boxes; A_o: surface of the open ocean

$$n = \tau \cdot T/V \tag{5}$$

with τ: ocean residence time of a tracer metal; T: transfer rate of water between the two boxes in km^3/kyr and:

$$s = \frac{S_o}{S} = \frac{a}{a + (1-a)\dfrac{rr_c}{rr_o}} \tag{6}$$

with rr_c: rain rate in the zone of high productivity in g/cm^2 kyr; rr_o: rain rate in the open ocean in g/cm^2 kyr; S: total flux of particles in g/kyr; S_o: total flux

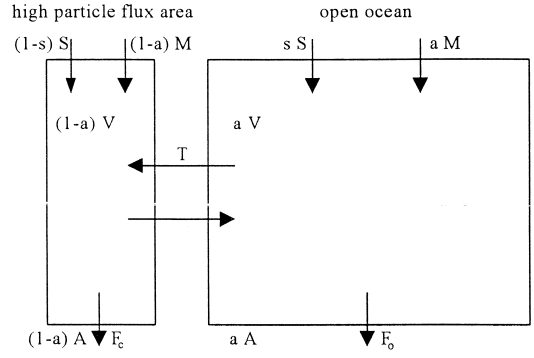

Fig. 7. Simple two-box model relating total flux of particles S [g/yr] and total flux of a tracer metal M [dpm/kyr] with water transfer rate T [km^3/kyr] and sediment flux densities of the metal [dpm/cm^2 kyr] according to Broecker and Peng (1982) and Rutsch et al. (1995). The abbreviations are explained in the text.

of particles of the open ocean in g/kyr; M: total flux of a tracer metal in dpm/kyr, with $M_{Pa}/M_{Th} = 0.093$.

The ratio R_{Pa}/R_{Th} describes how the flux of ^{231}Pa is enhanced in comparison to the flux of ^{230}Th (Eq. (7)), whereas the F_{cPa}/F_{cTh} ratio (Eq. (8)) corresponds to the measured $^{231}Pa_{ex}/^{230}Th_{ex}$ ratio in the SOC sediment. It can be shown that the maximal ratios of R_{Pa}/R_{Th} and F_{cPa}/F_{cTh} are functions of the ratios a, τ_{Pa}/τ_{Th} and rr_c/rr_o according to the following equations:

$$\frac{R_{pa}}{R_{Th}} = \frac{1+\dfrac{n_{Th}\dfrac{\tau_{pa}}{\tau_{Th}}}{(1-a)s}}{1+\dfrac{n_{Th}\dfrac{\tau_{pa}}{\tau_{Th}}}{(1-s)a}} \cdot \frac{1+\dfrac{n_{Th}}{(1-s)a}}{1+\dfrac{n_{Th}}{(1-a)s}} \tag{7}$$

$$\frac{F_{cPa}}{F_{cTh}} = \frac{M_{pa}}{M_{Th}} \cdot \frac{1+\dfrac{n_{Th}\dfrac{\tau_{pa}}{\tau_{Th}}}{(1-a)s}}{1+\dfrac{n_{Th}\dfrac{\tau_{pa}}{\tau_{Th}}}{(1-s)s}} \cdot \frac{1+\dfrac{n_{Th}}{(1-s)s}}{1+\dfrac{n_{Th}}{(1-a)s}} \tag{8}$$

To find the maximal values:

$$d\frac{\dfrac{R_{pa}}{R_{Th}}}{dn_{Th}} = 0 \tag{9}$$

and:

$$d\frac{\dfrac{F_{cPa}}{F_{cTh}}}{dn_{Th}} = 0 \tag{10}$$

Assuming $V = \text{const.}$, $\frac{\tau_{Pa}}{\tau_{Th}} \neq 1$ and $s \neq a$, the extreme values are for R_{Pa}/R_{Th}:

$$n_{Th(max)} = \pm\sqrt{\frac{as(s-1)(a-1)}{\dfrac{\tau_{Pa}}{\tau_{Th}}}} \tag{11}$$

with s expressed according to Eq. (6) the extreme R_{Pa}/R_{Th} ratio then results as:

$$\frac{R_{Pa}}{R_{Th(max)}} = \left(\frac{1+\sqrt{\dfrac{rr_c\tau_{Pa}}{rr_o\tau_{Th}}}}{\sqrt{\dfrac{\tau_{Pa}}{\tau_{Th}}}+\sqrt{\dfrac{rr_c}{rr_o}}}\right)^2 \tag{12}$$

and for F_{cPa}/F_{cTh}:

$$n_{Th(max)} = \pm s\sqrt{\frac{(s-1)(a-1)}{\dfrac{\tau_{Pa}}{\tau_{Th}}}} \tag{13}$$

with:

$$\frac{F_{cPa}}{F_{cTh(max)}} = \frac{M_{Pa}}{M_{Th}}\left(\frac{\sqrt{\dfrac{\tau_{Pa}}{\tau_{Th}}}+\sqrt{a\dfrac{rr_o}{rr_c}+(1-a)}}{1+\sqrt{\dfrac{\tau_{Pa}}{\tau_{Th}}\left(a\dfrac{rr_o}{rr_c}+(1-a)\right)}}\right)^2 \tag{14}$$

Maximum initial SOC $^{231}Pa_{ex}/^{230}Th_{ex}$ ratios derived from this function (14) are given in Fig. 6 for three different ratios of τ_{Pa}/τ_{Th} together with the data from a number of sediment cores from the area ($a = 0.66$). The model calculations correspond quite well with the observed ratios (Fig. 6, Table 5) with the exception of some of the sediment sections including stages 2 and 4 of core 2499-5 which were dominated by high opal rain rates where enhanced ^{231}Pa scavenging took place. These results suggest

Table 5
Calculated (Eq. (14)) maximal R_{Pa}/R_{Th} and F_{cPa}/F_{cTh} ratios, resulting from the two-box model calculation with $a = 0.66$, $\tau_{Pa}/\tau_{Th} = 10$ and $rr_o = 1$ g/cm^2 kyr

rr_c (g/cm^2 kyr)	R_{Pa}/R_{Th}	F_{cPa}/F_{cTh}
2	1.43	0.114
2.5	1.60	0.121
3	1.75	0.125
3.5	1.89	0.129
5	2.24	0.137

that our simple model describing the boundary scavenging of ^{231}Pa and sediment accumulation in the SOC of the Southern Ocean is realistic. Further applications of this model are discussed below.

5. The glacial scenario

During the glacial isotope stages 2 and 4 the $^{231}Pa_{ex}/^{230}Th_{ex}$ ratio of the PS2499-5 core was about double that expected from production (interglacials). Various investigations applying different methods have demonstrated a glacial northward shift of the high particle flux areas and possibly also the frontal system in this part of the Southern Ocean (Charles et al., 1991; Mortlock et al., 1991; Kumar et al., 1993, 1995; Frank et al., 1996). The area of high biogenic opal fluxes and high export productivity is presently located south of the APF in the Antarctic Zone of the ACC (Fig. 1). During glacials this area was located above or slightly north of the position of sediment core PS2499-5, as indicated by the $^{231}Pa_{ex}/^{230}Th_{ex}$ ratios but also the change in lithology from interglacial carbonate sedimentation to glacial biogenic opal sedimentation. The $^{231}Pa_{ex}/^{230}Th_{ex}$ ratios during the glacial stages are comparable with the ratios determined on sediment samples of isotope stage 1 recovered south of the present-day position of the APF (Kumar et al., 1993, 1995; Yu et al., 1996). The bulk rain rates and lithology of core PS2498-1 which is dominated by the accumulation of biogenic carbonate above the lysocline, clearly imply that the high opal flux area did not reach the position of this core during the last 130 kyr. It follows that the maximum glacial northward shift of the area of high biogenic particle flux, possibly together with the APF, in this area amounted to about 5°.

Additionally, the total width of the glacial zone of high productivity may be deduced using data from Kumar et al. (1995). The records of cores PS2499-5, RC13-254 and RC15-93 reveal an increased glacial particle flux and an increased $^{231}Pa_{ex}/^{230}Th_{ex}$ ratio, in contrast to the PS2498-1 and RC13-271 cores (Fig. 1, Table 4). Hence, the positions of the latter two cores limit the zone's maximum latitudinal width to about 6° (44°S–50°S) assuming a glacial northward shift of the high productivity zone and possibly also the frontal system as a consequence of the extended sea ice. The longitudinal width in the Atlantic sector of the Southern Ocean is supposed to be about 70°. Resulting is a total area of 3.5×10^6 km^2, equivalent to 4.7% of the Atlantic Ocean's surface of 7.42×10^7 km^2 (Keir, 1988) and equivalent to 10.9% of the Southern Ocean's surface of 3.2×10^7 km^2. This is essentially in agreement with the estimates used by Yu et al. (1996).

Assuming an average bulk rain rate of about 3.0 g/cm^2 kyr for the high opal productivity area, an average initial $^{231}Pa_{ex}$ activity of 0.8 dpm/g and an average water depth of 3.8 km, a total ^{231}Pa flux of 2.4 dpm/cm^2 kyr during the glacial stage 2 results. Comparing the average $^{231}Pa_{ex}/^{230}Th_{ex}$ ratio of 0.20 during the stage 2, from PS2499-5 and 3 cores from Yu et al. (1996), with the production ratio of 0.093, the total $^{231}Pa_{ex}$ flux of 2.4 dpm/cm^2 kyr represents 215% of the produced $^{231}Pa_{ex}$ in this area. Hence, there was an additional $^{231}Pa_{ex}$ flux of 1.28 dpm/cm^2 kyr. According to the calculated surface of 3.5×10^6 km^2, an additional $^{231}Pa_{ex}$ flux of 4.5×10^{16} dpm/kyr results. For the glacial stage 4 a similar additional $^{231}Pa_{ex}$ flux results when the same surface area is assumed. This additional $^{231}Pa_{ex}$ flux in the glacial zone of high productivity represents about 8% of the total ^{231}Pa produced in the Atlantic Ocean (assumed surface of about 6.3×10^7 km^2, Atlantic Ocean without Atlantic Sector of Southern Ocean, average depth of 3.8 km).

The evaluation of ^{231}Pa deposition in the remaining area of the Southern Ocean is more uncertain. Applying the average $^{231}Pa_{ex}/^{230}Th_{ex}$ ratio of 0.14 $\pm$ 0.02 given by Yu et al. (1996) and a rain rate value of 2.5 g/cm^2 kyr yields a depositional flux of 2 dpm/cm^2 kyr, of which 0.67 dpm/cm^2 kyr, calculated as: 2 dpm/cm^2 kyr $\times (1 - 0.093/0.14)$, are imported into the Southern Ocean. This flux times an area of 2.85×10^7 km^2 (derived as $3.2 \times 10^7 - 3.5 \times 10^6$ km^2) yields an import of ^{231}Pa of 1.91×10^{14} dpm/yr. Together with the import of ^{231}Pa in the zone of high productivity of 4.5×10^{13} dpm/yr a total import of 2.36×10^{14} dpm/yr results which amounts to about 42% of the total ^{231}Pa produced in the Atlantic Ocean (without Atlantic sector of Southern Ocean). This corroborates the previous estimations by Yu et al. (1996).

6. Sensitivity of $^{231}Pa_{ex}/^{230}Th_{ex}$ in Southern Ocean sediments to changes of deep water circulation

In order to test how sensitive the $^{231}Pa_{ex}/^{230}Th_{ex}$ activity ratio and the import flux of ^{231}Pa into Southern Ocean sediments react to changes of deep water circulation the trace metal's flux density in the SOC F_c is expressed according to Rutsch et al. (1995) as:

$$F_c = \frac{M}{A}\frac{1+\dfrac{n}{(1-a)\,s}}{1+\dfrac{n}{(1-s)\,s}} = \frac{M}{A}\frac{1+\dfrac{a\tau}{(1-a)\,st_{water}}}{1+\dfrac{a\tau}{(1-s)\,st_{water}}} \quad (15)$$

Assuming constant ratios of M/A, a, s and constant V and τ, the flux density is a function of residence time of ocean water masses, $t_{water} = V_o/T = aV/T = a\tau/n$. Fig. 8 shows the resulting functions for ^{230}Th and ^{231}Pa, respectively. In this model F_{cPa}, F_{cTh} and the ratio F_{cPa}/F_{cTh} (dashed line) are not very sensitive to changes in water residence time.

Additionally, we run a balance in which the import fluxes of ^{230}Th and ^{231}Pa are determined by the flux of NADW into the Southern Ocean, for comparison with the results of Yu et al. (1996). The total yearly depositional fluxes D of ^{231}Pa and of $^{230}Th_{ex}$ are evaluated as:

$$D = \left(TC_{(t)}\right) + \beta V_{SOC} \quad (16)$$

with t_{water}: age of the NADW arriving at the SOC, $t_{water} = V_o/T = aV/T = a\tau/n$; T: transfer rate of water into the SOC; $C_{(t)}$: concentration of ^{231}Pa or ^{230}Th in the open deep Atlantic Ocean depending on t_{water}; β: production rate of ^{231}Pa and ^{230}Th in the SOC

with:

$$C_{(t)} = \beta\tau\left(1 - e^{-t/\tau}\right) \quad (17)$$

We used for $C_{(t)}$, β, V_o, and V_{SOC} the same values as Yu et al. (1996) of, respectively, 2.33×10^{-3} dpm/m^3 yr, 2.52×10^{-2} dpm/m^3 yr, 2.39×10^{17} m^3 and 1.22×10^{17} m^3.

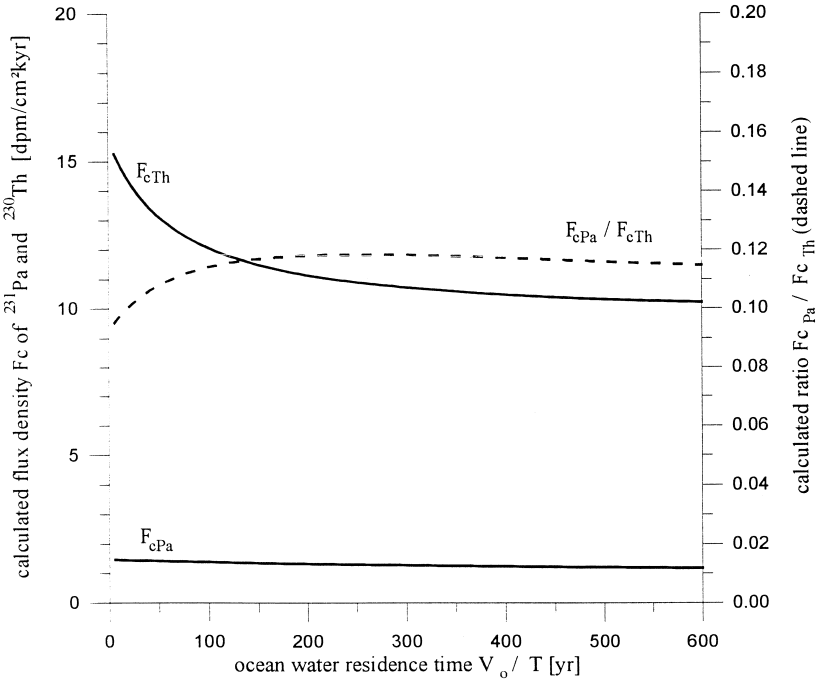

Fig. 8. Calculated flux densities F_c of ^{231}Pa and ^{230}Th according to the two-box model (Eq. (15)) with a = 0.66; s = 0.44; $\tau_{Th} = 25$ yr; $\tau_{Pa} = 220$ yr; $M_{Pa}/A = 0.885$ dpm/cm^2 kyr; $M_{Th}/A = 9.576$ dpm/cm^2 kyr. The abbreviations are explained in the text.

The results for different residence times of NADW between 100 and 600 years (column 1) are listed in Table 6. Columns 2 and 4 show the total depositional fluxes of ^{231}Pa and ^{230}Th [dpm/yr] together with the fraction of Atlantic ^{231}Pa and ^{230}Th advected into the southern ocean (columns 3 and 5). Finally, column 6 lists the activity ratio of $^{231}Pa_{ex}/^{230}Th_{ex}$ of the SOC sediments resulting from the total fluxes (import from the Atlantic plus in situ production). The evaluation by Yu et al. (1996) corresponds to a residence time of the water of 180 years, and yields an ADV of 0.68 for ^{231}Pa and 0.14 for ^{230}Th, and a $^{231}Pa_{ex}/^{230}Th_{ex}$ activity ratio of 0.17. As can be seen in the next columns a doubling of the residence time of deep water lowers the activity ratio in the sediments to 0.16. Thus this estimate confirms the results of the previous model suggesting that the activity ratio in the SOC is *not* very sensitive to circulation changes. A slower circulation (360 years) lowers the ^{231}Pa flux into Southern Ocean sediments to about 84% of the one during faster circulation (180 years), whereas ^{230}Th would be less sensitive (89%). Because of the large uncertainty of the average values for the glacial activity ratio of the SOC sediments (at least ± 0.02) and of the value for the import of ^{231}Pa from the Atlantic (estimated to be at least $\pm 30\%$), the conclusion is that neither the flux of ^{231}Pa nor the $^{231}Pa_{ex}/^{230}Th_{ex}$ ratio in SOC sediments are reliable proxies for changes in ocean circulation. The similarity between the glacial and the Holocene SOC sediments does not exclude significant changes of production of NADW in the past.

Table 6
Calculated balance of the ^{231}Pa and ^{230}Th deposition south of the APF as function of changes in the water residence time in the Atlantic and Southern Oceans, $\tau_{Pa} = 220$ yr and $\tau_{Th} = 25$ yr

Water residence time t [yr]	Total flux ^{231}Pa [dpm/yr]	ADV_{Pa}	Total flux ^{230}Th [dpm/yr]	ADV_{Th}	$^{231}Pa/^{230}Th$
100	7.31E+14	0.80	4.55E+15	0.25	0.16
120	7.13E+14	0.77	4.31E+15	0.21	0.17
140	6.96E+14	0.74	4.14E+15	0.18	0.17
160	6.8E+14	0.71	4.01E+15	0.16	0.17
180	6.64E+14	0.68	3.91E+15	0.14	0.17
200	6.5E+14	0.66	3.82E+15	0.12	0.17
220	6.36E+14	0.63	3.75E+15	0.11	0.17
240	6.23E+14	0.61	3.7E+15	0.10	0.17
260	6.11E+14	0.59	3.65E+15	0.10	0.17
280	5.99E+14	0.57	3.61E+15	0.09	0.17
300	5.88E+14	0.55	3.57E+15	0.08	0.16
320	5.77E+14	0.53	3.54E+15	0.08	0.16
340	5.68E+14	0.51	3.51E+15	0.07	0.16
360	5.58E+14	0.49	3.49E+15	0.07	0.16
380	5.49E+14	0.48	3.47E+15	0.07	0.16
400	5.41E+14	0.46	3.45E+15	0.06	0.16
420	5.32E+14	0.45	3.43E+15	0.06	0.16
440	5.25E+14	0.43	3.41E+15	0.06	0.15
460	5.17E+14	0.42	3.4E+15	0.05	0.15
480	5.1E+14	0.41	3.38E+15	0.05	0.15
500	5.04E+14	0.39	3.37E+15	0.05	0.15
520	4.97E+14	0.38	3.36E+15	0.05	0.15
540	4.91E+14	0.37	3.35E+15	0.05	0.15
560	4.86E+14	0.36	3.34E+15	0.04	0.15
580	4.8E+14	0.35	3.33E+15	0.04	0.14
600	4.75E+14	0.34	3.32E+15	0.04	0.14

7. Conclusions

The sediments of two locations, one north and one south of the present position of the Subantarctic Front, have been strongly influenced by variable bottom current-induced sediment focussing during the last 130 kyr. Correction for these sediment redistribution effects yielded pronounced maxima of opal-dominated sediment rain rates during glacial stages 2 and 4 in the southern core whereas no significant variations are recorded at the northern location. These variations in particle flux and its composition in the southern core have also been recorded by the $^{231}Pa_{ex}/^{230}Th_{ex}$ ratio, which is well independent of sediment redistribution. We infer from these results that the high opal productivity area presently located south of the APF was shifted northwards to at least the position of the sediment core PS2499-5, but not until the position of PS2498-1, 2° further north, during the glacial stages 2 and 4. This limits the glacial northward shift of the high opal productivity area, and possibly also the APF itself, to a maximum of about 5 degrees.

Modelling of the particle fluxes, the $^{231}Pa_{ex}/^{230}Th_{ex}$ ratios and the boundary scavenging intensity in the Atlantic sector of the Southern Ocean applying a simple two-box model constrains the maximum possible $^{231}Pa_{ex}/^{230}Th_{ex}$ values which can be related to increased particle fluxes. The model reveals that the total ^{231}Pa flux and the $^{231}Pa_{ex}/^{230}Th_{ex}$

activity ratio have not been very sensitive to changes of water mass residence times (e.g., NADW) in the Atlantic Ocean. We conclude from this that it is probably not possible to exclude from Southern Ocean $^{231}Pa_{ex}/^{230}Th_{ex}$ data that significant changes of NADW production have occurred on glacial/interglacial time scales.

Acknowledgements

We are grateful to Roger Francois and an anonymous reviewer for constructive criticism. This work was supported by the German Science Foundation (DFG), Grant Ma821/9-3. This is AWI-publication No. 1522 and SFB 261 publication No. 266.

References

Anderson, R.F., Bacon, M.P., Brewer, P.G., 1983. Removal of ^{230}Th and ^{231}Pa from the open ocean. Earth Planet. Sci. Lett. 62, 7–23.

Anderson, R.F., Lao, Y., Broecker, W.S., Trumbore, S.E., Hofmann, H.J., Wölfli, W., 1990. Boundary scavenging in the Pacific Ocean: a comparison of ^{10}Be and ^{231}Pa. Earth Planet. Sci. Lett. 96, 287–304.

Anderson, R.F., Fleisher, M.Q., Biscaye, P.E., Kumar, N., Dittrich, B., Kubik, P., Suter, M., 1994. Anomalous boundary scavenging in the Middle Atlantic Bight: evidence from ^{230}Th, ^{231}Pa, ^{10}Be and ^{210}Pb. Deep-Sea Research II 41, 537–561.

Bacon, M.P., Anderson, R.F., 1982. Distribution of thorium isotopes between dissolved and particulate forms in the deep-sea. J. Geophys. Res. 87, 2045–2056.

Boyle, E.A., 1988. Cadmium: chemical tracer of deep-water paleoceanography. Paleoceanography 3, 471–489.

Broecker, W.S., Peng, T.-H., 1982. Tracers in the Sea, Eldigo, New York.

Charles, C.D., Fairbanks, R.G., 1990. Glacial to interglacial changes in the isotopic gradients of the Southern Ocean surface water. In: Bleil, U., Thiede, J. (Eds.), Geological History of the Polar Oceans: Arctic versus Antarctic, Kluwer Academic, Norwell, MA, pp. 519–538.

Charles, C.D., Froehlich, P.N., Zibello, A., Mortlock, R.A., Morley, J.J., 1991. Biogenic opal in Southern Ocean sediments over the last 450,000 years: implications for surface water chemistry and circulation. Paleoceanography 6, 697–728.

Francois, R., Bacon, M.P., Altabet, M.A., Labeyrie, L.D., 1993. Glacial/interglacial changes in sediment rain rate in the SW Indian sector of Subantarctic waters as recorded by ^{230}Th, ^{231}Pa, U and δ^{15}N. Paleoceanography 8, 611–629.

Francois, R., Altabet, M.A., Yu, E.-F., Sigman, D., Bacon, M.P., Frank, M., Bohrmann, G., Bareille, G., Labeyrie, L.D., 1997. Contribution of Southern Ocean surface-water stratification to low atmospheric CO_2 concentrations during the last glacial period. Nature 389, 929–935.

Frank, M., 1996. Reconstruction of Late Quaternary environmental conditions applying the natural radionuclides ^{230}Th, ^{10}Be, ^{231}Pa and ^{238}U: a study of deep-sea sediments from the eastern sector of the Antarctic Circumpolar Current System. Ber. Polarforsch., p. 186.

Frank, M., Eckhardt, J.-D., Eisenhauer, A., Kubik, P.W., Dittrich-Hannen, B., Mangini, A., 1994. ^{10}Be, ^{230}Th and ^{231}Pa in Galapagos Microplate sediments: implications for hydrothermal activity and paleoproductivity changes during the last 100,000 years. Paleoceanography 9, 559–578.

Frank, M., Gersonde, R., Rutgers van der Loeff, M.M., Kuhn, G., Mangini, A., 1996. Late Quaternary sediment dating and quantification of lateral sediment redistribution applying $^{230}Th_{ex}$: a study from the eastern Atlantic sector of the Southern Ocean. Geol. Rundsch. 85, 554–566.

Frank, N., Mangini, A., 1995. A simplified procedure for the measurement of ^{231}Pa in Mn encrustations. Nucl. Instrum. Meth. Phys. Res. B 101, 258–262.

Gersonde, R., 1995. Die Expedition ANTARKTIS-XI/2 mit FS 'Polarstern' 1993/94. Ber. Polarforsch., 163.

Keir, R.S., 1988. On the late Pleistocene Ocean geochemistry and circulation. Paleoceanography 3, 413–445.

Kumar, N., Gwiazda, R., Anderson, R.F., Froehlich, P.N., 1993. $^{231}Pa/^{230}Th$ ratios in sediments as a proxy for past changes in Southern Ocean productivity. Nature 362, 45–48.

Kumar, N., Anderson, R.F., Mortlock, R.A., Froehlich, P.N., Kubik, P., Dittrich-Hannen, B., Suter, M., 1995. Increased biological productivity and export production in the glacial Southern Ocean. Nature 378, 675–680.

Luo, S., Ku, T.L., 1996. $^{231}Pa/^{230}Th$ Ratios as Particle-Flux Proxy; Influence of Particle Composition. Abstr. AGU Fall Meeting EOS 77, F320.

Mangini, A., Sonntag, C., Bertsch, G., Müller, E., 1979. Evidence for a higher natural U-content in world rivers. Nature 79, 337–339.

Mortlock, R.A., Charles, C.D., Froehlich, P.N., Zibello, M.A., Saltzman, J., Hays, J.D., Burckle, L.H., 1991. Evidence for lower productivity in the Antarctic Ocean during the last glaciation. Nature 351, 220–223.

Nozaki, Y., Horibe, Y., Tsubota, H., 1981. The water column distribution of thorium isotopes in the western North Pacific. Earth Planet. Sci. Lett. 54, 203–216.

Peterson, R.G., Stramma, L., 1991. Upper-level circulation in the South Atlantic Ocean. Progress in Oceanography 26, 1–73.

Rutgers van der Loeff, M.M., Berger, G.W., 1993. Scavenging of ^{230}Th and ^{231}Pa near the Antarctic Polar Front in the South Atlantic. Deep-Sea Research I 40, 339–357.

Rutsch, H.-J., Mangini, A., Bonani, G., Dittrich-Hannen, B., Kubik, P.W., Suter, M., Segl, M., 1995. ^{10}Be and Ba concentrations in West African sediments trace productivity in the past. Earth Planet. Sci. Lett. 133, 129–143.

Sea Ice Climatic Atlas, Vol. 1, Antarctica, 1985. Naval Oceanography Command Detachment, Ashville, NC.

Spencer, D.W., Bacon, M.P., Brewer, P.G., 1981. Models of the distribution of ^{210}Pb in a section across the north equatorial Atlantic Ocean. J. Mar. Res. 39, 119–138.

Walter, H.J., Rutgers van der Loeff, M.M., Hoeltzen, H., 1997. Enhanced scavenging of ^{231}Pa relative to ^{230}Th in the South Atlantic south of the Polar Front. Implications for the use of the ^{231}Pa/^{230}Th ratio as a paleoproductivity proxy. Earth Planet. Sci. Lett. 149, 85–100.

Yu, E.-F., Francois, R., Bacon, M.P., 1996. Similar rates of modern and last-glacial ocean thermohaline circulation inferred from radiochemical data. Nature 379, 689–694.